ACS Catalysis

Research Article

pubs.acs.org/acscatalysis

Effect of Cage Size on the Selective Conversion of Methanol to Light Olefins

Yashodhan Bhawe,[†] Manuel Moliner-Marin,[†,⊥] Jonathan D. Lunn,[‡] Yu Liu,[§] Andrzej Malek,[‡] and Mark Davis*[,†]

[†]Chemical Engineering, California Institute of Technology, Pasadena, California 91125, United States

[‡]Inorganic Materials & Heterogeneous Catalysis, The Dow Chemical Company, Midland Michigan 48640, United States

[§]Hydrocarbon and Energy R&D, The Dow Chemical Company, Freeport Texas 77541, United States

Supporting Information

ABSTRACT: Zeolites that contain eight-membered ring pores but different cavity geometries (LEV, CHA, and AFX structure types) are synthesized at similar Si/Al ratios and crystal sizes. These materials are tested as catalysts for the selective conversion of methanol to light olefins. At 400 °C, atmospheric pressure, and 100% conversion of methanol, the ethylene selectivity decreases as the cage size increases. Variations in the Si/Al ratio of the LEV and CHA show that the maximum selectivity occurs at Si/Al = 15−18. Because lower Si/Al ratios tend to produce faster deactivation rates and poorer selectivities, reactivity comparisons between frameworks are performed with solids having a ratio Si/Al = 15−18. With LEV and AFX, the data are the first from materials with this high Si/Al. At similar Si/Al and primary crystallite size, the propylene selectivity for the material with the CHA structure exceeds those from either the LEV or AFX structure. The AFX material gives the shortest reaction lifetime, but has the lowest amount of carbonaceous residue after reaction. Thus, there appears to be an intermediate cage size for maximizing the production of light olefins and propylene selectivities equivalent to or exceeding ethylene selectivities.

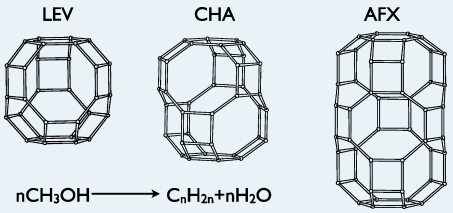

KEYWORDS: *methanol-to-olefins, zeolite, CHA, LEV, AFX*

1. INTRODUCTION

The methanol-to-olefins (MTO) reaction can be accomplished using solid acid catalysts, such as zeolites (aluminosilicates) and silicoaluminophosphates (SAPOs), and is an industrially viable method for the conversion of methanol to light olefins at temperatures above 350 °C. This reaction provides a route for the production of light olefins from nonpetroleum sources such as natural gas, coal, and biomass by using methanol as an intermediate. SAPO-34,[1] a silicoaluminophosphate with the chabazite (CHA) topology (three-dimensional cage structure with 8-membered ring (8MR) pores), is one of the most studied catalysts for this reaction[2] and is the first molecular sieve commercialized for this process.[3]

A proposed mechanism for the MTO reaction involves the formation of a "hydrocarbon pool"[2] of substituted aromatic molecules[4] that are critical to the formation of light olefins by side chain reactions.[5] Conversion of methanol to olefins does not require a cage structure, and it can take place in channel pore structures (e.g., MFI[6]); however, small pore framework cages are effective in retaining these reactive intermediates and, thus, limiting the overall process selectivity to lighter, nonaromatic products only.[7] In addition to SAPO's, zeolites of similar topology (e.g., SSZ-13[8]) can be utilized to catalyze this reaction. To date, the effect of cage size on the selective conversion of methanol to light olefins has not been well studied.[9]

Here, we focus on how the size of a zeolite cage can affect the conversion of methanol and the selectivity toward ethylene and propylene production. We investigated zeolites with the LEV, CHA, and AFX frameworks because all three topologies have cages that are accessed by 8MR pores (schematics of topologies are provided in Figure 1[10]). Previous work has revealed that variations in crystal

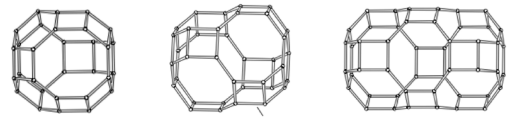

Pore Size	4.8Å*3.6Å	3.8Å * 3.8Å	3.4Å*3.6Å
Cage Dimensions	8.05Å*8.05Å *6.95Å	8.35Å*8.35Å *8.23Å	8.35Å*8.34Å *13.03Å

Figure 1. Cages studied and their dimensions. Figures and dimensions obtained from the Atlas of Zeolite Framework Types.[10]

parameters, such as Al content in the zeolite,[11,12] and crystallite size[7] can alter the reactivity. Thus, care was taken to keep all crystal parameters constant across the catalysts studied here. This allowed for the elucidation of the effect of framework topology alone on the selectivities in the MTO reaction. Once these effects were determined, we investigated the effects of cage size over a range of Si/Al ratios with small crystallite sizes.

Received: August 21, 2012
Revised: October 5, 2012
Published: October 18, 2012

 © 2012 American Chemical Society dx.doi.org/10.1021/cs300558x | *ACS Catal.* 2012, 2, 2490−2495

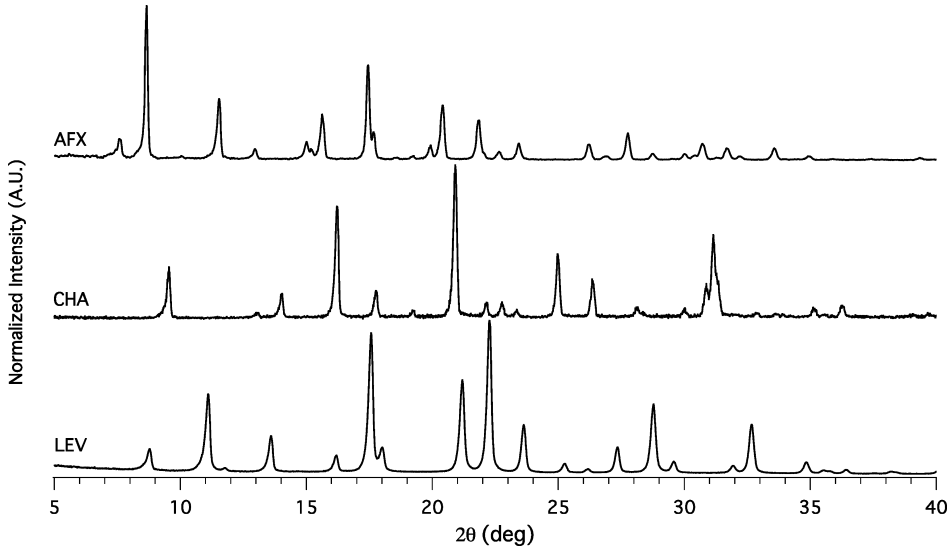

Figure 2. XRD patterns of as-made crystallized zeolites.

Table 1. Characterizations and Reaction Data for Zeolites

framework	Si/Al	aggregate crystal size (μm)	primary crystallite size (Å)	maximum $C_{3=}$ selectivity	maximum $C_{2=}$ selectivity	maximum (C_2 + C_3) selectivity
LEV	16.8	1−3	389	32	43	69
CHA	14.4	1−3	364	44	46	79
AFX	16.7	3−5	395	31	23	53

2. EXPERIMENTAL SECTION

2.1. Organic Structure Directing Agents. The organic structure-directing agents (SDAs) required for the zeolite syntheses were prepared in-house. The LEV material was obtained using a *N*-methylquinuclidinium hydroxide SDA.[13] The CHA material was synthesized with the *N*,*N*,*N*-trimethyladamantylammonium hydroxide SDA.[8] The AFX material was crystallized using the 1,3-bis(1-adamantyl)imidazolium hydroxide SDA as described by Archer et al.[14]

2.2. Inorganic Synthesis. Syntheses used to yield materials of desired crystal Si/Al were modified from known recipes.[13,8,14]

LEV (SSZ-17): A synthesis gel of the composition $1SiO_2$/$0.023Al_2O_3$/0.2ROH/0.2NaOH/$40H_2O$ was prepared with Cabosil M5 as the silica source, Reheis F2000 as the alumina source, and Baker NaOH pellets as the NaOH source (ROH is the SDA). The gel was loaded into a Teflon-lined autoclave and heated under autogenous pressure at 170 °C with tumbling. After 6 days, a crystalline product was recovered, washed with water, and dried.

CHA (SSZ-13): A synthesis gel of the composition $1SiO_2$/$0.026Al_2O_3$/0.2ROH/0.2NaOH/$40H_2O$ was prepared with Cabosil M5 as the silica source, Reheis F2000 as the alumina source, and Baker NaOH pellets as the NaOH source. The gel was loaded into a Teflon-lined autoclave and heated under autogenous pressure at 160 °C with tumbling. After 5 days, a crystalline product was recovered, washed with water, and dried.

AFX (SSZ-16): A synthesis gel of the composition $1SiO_2$/$0.028Al_2O_3$/0.25ROH/0.1NaOH/$30H_2O$ was prepared with Cabosil M5 as the silica source, Tosoh HSZ320NAA as the Al source, and Baker NaOH pellets as the NaOH source. The gel was loaded into a Teflon-lined autoclave and heated under autogenous pressure at 150 °C with tumbling. After 12 days, a crystalline product was recovered, washed with water, and dried.

2.3. Si/Al Variation of the Zeolites. To vary the Si/Al of the structures studied, two different approaches were used. For the CHA and LEV frameworks, compositional variations could be achieved by changing the amount of $Al(OH)_3$ added to the synthesis gel. The AFX framework was not amenable to incorporating more aluminum using the same recipe. For the high-aluminum SSZ-16 material, an alternative literature recipe[15] was employed.

2.4. Characterization. The as-made materials were characterized by powder X-ray diffraction (XRD) on a Rigaku Miniflex II diffractometer with Cu K_α radiation to determine structure type and purity. The primary crystallite sizes were determined by X-ray line broadening using the Scherrer equation[16] assuming an equivalent spherical particle. Thermogravimetric analyses (TGA) were conducted on a Netzsch STA-449C Jupiter instrument. Thermogravimetric analysis was used to determine the calcined, dry weight per mass of loaded catalyst. Scanning electron microscopy/energy dispersive spectropscopy (SEM/EDS) analyses were conducted on a JEOL JSM-6700F instrument equipped with an Oxford INCA Energy 300 X-ray energy dispersive spectrometer. The SEM/EDS was used to determine the morphology and aggregate sizes and the Si/Al of the zeolites.

2.5. Reaction Testing. Prior to reaction testing, all materials were calcined in medical grade air. The materials were heated to 150 °C at 1 °C/min under flowing air, held for 3 h under flowing air, then heated further to 580 °C at 1 °C/min and held for 10 h under flowing air. The materials were then exchanged three times with 1 M NH_4NO_3 at 95 °C for 2 h, after which they were washed with water and dried. The dried materials were then pelletized, crushed, and sieved. Particles between 0.6 mm and 0.18 mm were supported between glass wool beds in an Autoclave Engineers BTRS Jr. SS-316 tubular, continuous flow reactor. All catalysts were heated to 580 °C in situ in a 30 cm^3/min flow of 5% Ar/95% He for 4 h prior to the reaction. The reactions were conducted at 400 °C in a 10% methanol/inert flow. Methanol was introduced via a liquid syringe pump at 5.4 μL/min, into a gas stream of the inert blend at

dx.doi.org/10.1021/cs300558x | *ACS Catal.* 2012, 2, 2490−2495

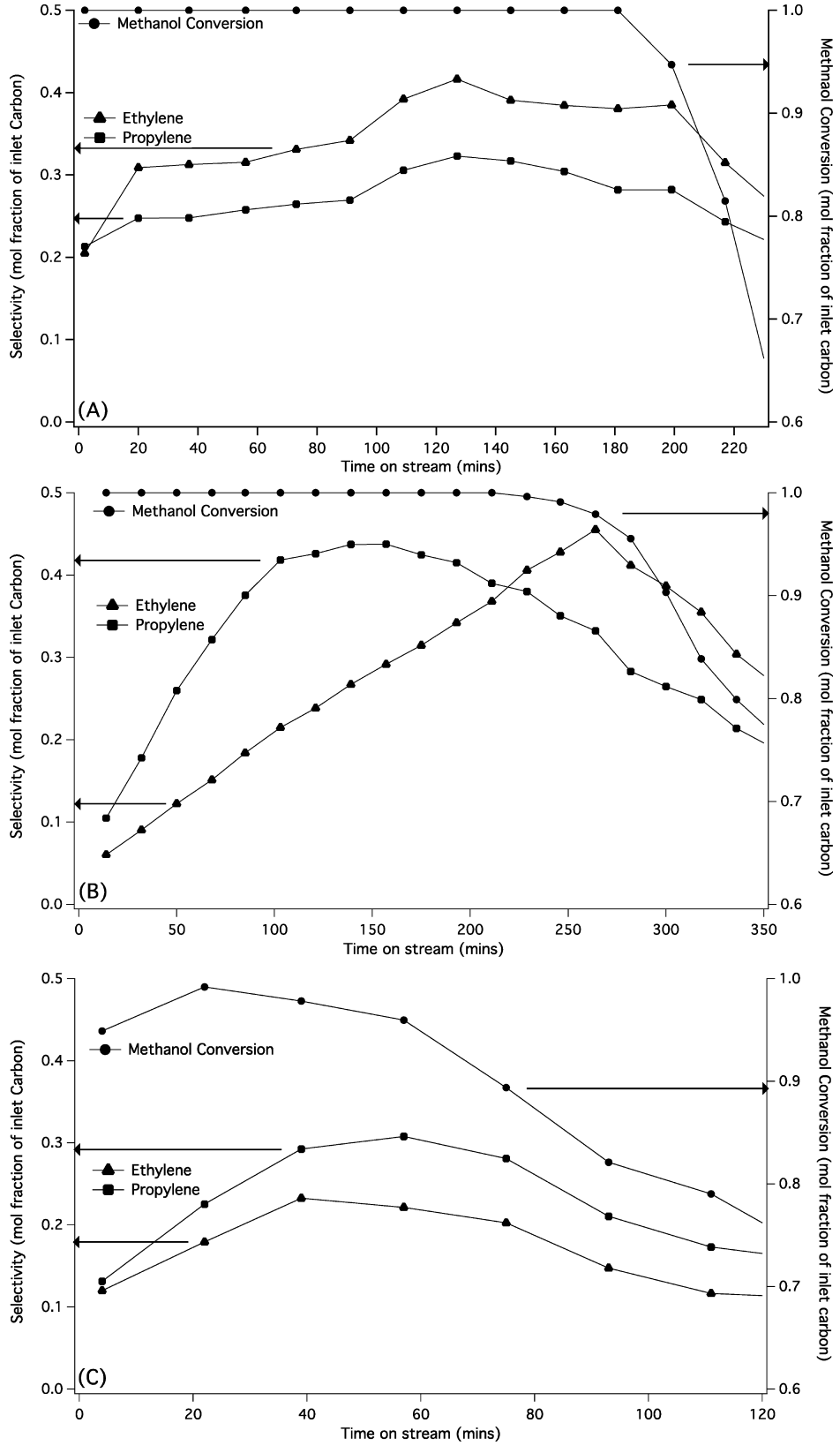

Figure 3. Representative time profiles of conversion, ethylene selectivity, and propylene selectivity for LEV (A), CHA (B), and AFX (C). Lines connect data points to guide the eye.

30 cm^3/min. The reactant flow had a weight hourly space velocity of 1.3 h^{-1}. In a typical run, 200 mg of dry catalyst was loaded. Effluent gases were evaluated using an on-stream GC/MS Agilent GC 6890/MSD5793N with a Plot-Q capillary column installed. Conversions and selectivities were computed on a carbon mole basis.

2.6. Occluded Organic Analysis. Occluded organics were extracted and isolated from spent zeolites through HF

dx.doi.org/10.1021/cs300558x | *ACS Catal.* 2012, 2, 2490−2495

dissolution and extraction into deuterated methylene chloride. Typically, 80 mg of spent zeolite was added to a 15 mL polypropylene centrifuge tube, followed by the addition of ~4 mL of deionized water and 2 mL of 48 wt % aqueous hydrofluoric acid. The dispersions were stirred for about 2 h to allow for complete framework dissolution. Following dissolution, the carbonaceous species were extracted twice into 2 mL of deuterated methylene chloride to permit solution NMR and GC/MS studies.

For the gas chromatography/mass spectrometry, 1−4 μL aliquots of the solution were injected into an Agilent 6890N. GC coupled to a Micromass GCT, SN CA095, TOF GC/MS system operating in the electron impact (EI) mode was used to obtain the mass spectra. Quantitative analyses were conducted by coupling the GC to an FID detector and matching the corresponding GC/MS results.

3. RESULTS AND DISCUSSION

3.1. Zeolite Catalysts. The synthesized zeolites were analyzed by powder XRD and SEM/EDS. The syntheses used here yielded pure crystals of the desired structure on the basis of comparisons of XRD patterns to reference patterns in the IZA database (Figure 2). The primary crystallite sizes were measured from the XRD data using the Scherrer equation, and the results show that the sizes of the primary crystallites for all the materials were between 350 and 400 Å (Table 1). SEM images reveal that the primary crystallites form aggregate solid particles that are ~1−5 μm in size (Table 1 and Supporting Information Figure S1). The AFX particles (3−5 μm) were slightly larger than the CHA and LEV particles (1−3 μm). EDS analyses of these materials yielded similar Si/Al ratios that were between 14 and 17. ^{27}Al and ^{29}Si MAS NMR spectra were obtained, and the data are consistent with no extra-crytalline materials being contained within the solid samples (Supporting Information Figure S2). A summary of the characterization data for the zeolites is shown in Table 1. From the data shown in Table 1, it is clear that these materials are appropriate for examining the effects of cage size on the selectivity to lower olefins in the MTO reaction while holding all other properties relatively constant.

Figure 3 illustrates the time-on-stream reaction data from the three different zeolites. These data show that the selectivity toward olefins increases over time when the conversion is at 100% but rapidly drops once the conversion begins to decrease below 80%. The conversions and selectivities for the AFX material rapidly decline after the 90 min on stream. Table 1 lists a summary of the reaction data for all three materials (the maximum ethylene, propylene, and maximum combined C_2−C_3 olefin selectivities for the three frameworks studied).

The most apparent trend in the reactivity data is that the maximum ethylene selectivity is higher for materials with smaller cages. The overall ethylene selectivities for LEV, CHA, and AFX are 33.8%, 28.4%, and 16.6%, respectively. These data suggest that smaller cages favor the formation of ethylene. The LEV material is the only catalyst that produces more ethylene than propylene after 90 min on-stream. The maximum propylene selectivity is the highest for CHA.

The AFX material has the shortest lifetime and the worst carbon balance of the three materials studied. It deactivates much faster than the CHA and LEV materials, and at most, 53% of the methanol feed is recovered in ethylene and propylene. The amount of carbonaceous material deposited on the catalyst samples during tests was determined from thermogravimetric analysis. Figure 4 shows TGA data obtained from spent samples of all three materials. AFX has the lowest amount of higher

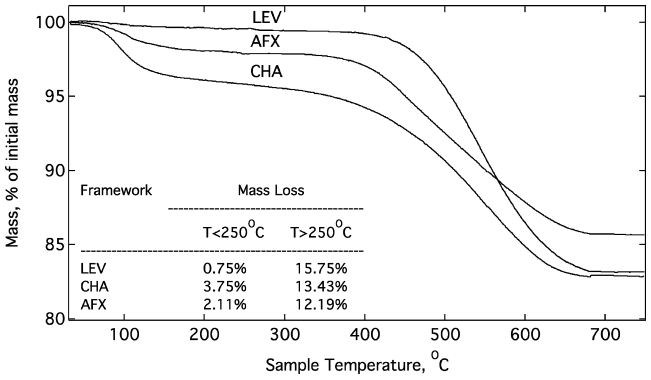

Figure 4. Thermogravimetric analysis data for zeolites with constant Si/Al after reaction. Samples were heated to 750 °C at 5 °C/min under a flow of air. "Low temp" mass loss was attributed to water removal, and "high temp", to organic combustion.

temperature mass loss, 1.3−3.5%, lower than CHA and LEV, respectively.

Occluded Organic Analysis. To understand the carbonaceous buildup during the reaction and at the end of the catalyst lifespan, analyses of the occluded organic species were conducted at the time of maximum propylene conversion (see Table 2 for time on-stream) and at the time of complete deactivation through HF dissolution of the zeolite framework. GC/MS data are presented in Figure 5 and the corresponding ^{1}H NMR and UV−vis spectra are shown in the Supporting Information (Figures S3−S5). The GC/MS distribution data in Figure 5 suggest that the carbonaceous species formed during the reaction are related to the size of the cavities present in the respective frameworks. The partially deactivated catalysts show that the size of the organics at maximum propylene selectivity correlate with the cage size (C2−benzenes for LEV; C3−C4−benzenes for CHA and C5−anthracenes for AFX). LEV and CHA also show a trend of forming light coked species first, and upon further deactivation, these light carbonaceous species (toluenes, xylenes, etc.) are converted to heavier carbonaceous species (higher alkylated benzenes and anthrones for LEV and alkylated napthalenes for CHA). As the reaction proceeds, alkyl substituents are added to the hydrocarbon pool, and upon the formation of some critical concentration of these polyaromatic species, the catalyst deactivates.

Table 2. Average Molecular Weights of Occluded Organics and Time of Removal from Reaction Stream for the Three Frameworks after Partial and Complete Deactivation

	partially deactivated		completely deactivated	
	time on stream (min)	av MW of organic material	time on-stream (min)	av MW of organic material
LEV	123	91	250	112
CHA	140	77	360	141
AFX	60	101	130	100

AFX, on the other hand, shows that larger organic species are formed first, and then the diminished remaining free cage volume is filled up with smaller organic molecules as the catalyst deactivates. This is seen in the increased organic content in the monoaromatic region upon complete deactivation that is absent in the partially coked material. This suggests that the mechanism for coking of the AFX cage is different from the mechanism for coking of the CHA and LEV materials. It suggests that the large anthracene-based molecules are formed relatively quickly in the

dx.doi.org/10.1021/cs300558x | ACS Catal. 2012, 2, 2490−2495

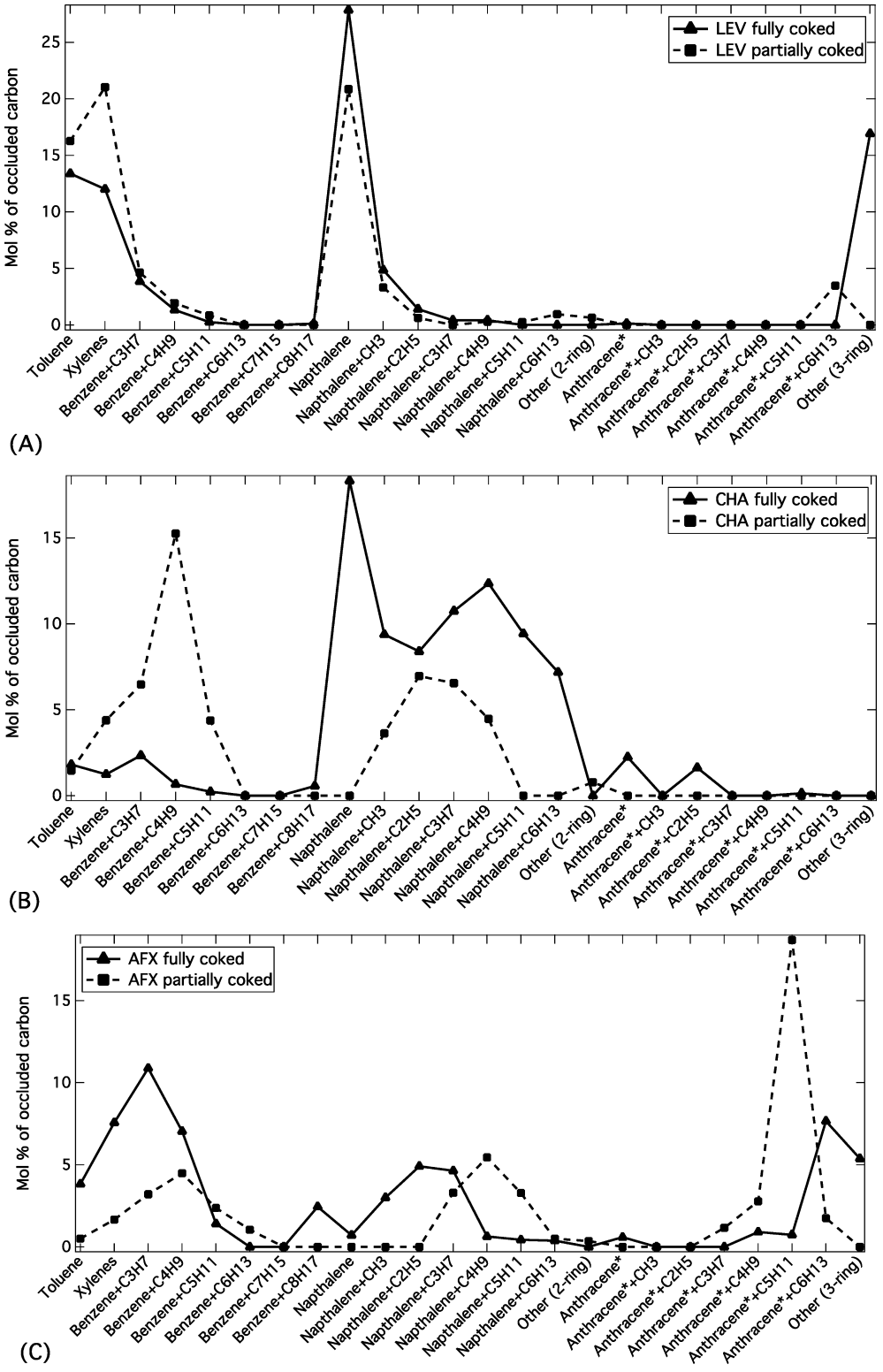

Figure 5. Occluded organic analyses of the catalysts stopped at maximum propylene conversion and after complete deactivation for LEV (A), CHA (B), and AFX (C). (Note: Anthracene* refers to anthracene or Phenanthrene.)

AFX cages as the hydrocarbon pool builds up. We did not observe the formation of any significant amounts of four-ring or larger aromatic rings. Instead, the still available free space is filled with single-ring aromatics and further alkylation products. Given the large size of these carbon pool molecules, the carbon balance is poor at the start of the reaction (42% by mol yield of C_1-C_4 in the first 2 data points). However, upon formation of these anthracene species, further growth of aromatic structure is impaired. This hypothesis can be supported by estimating the volume of the larger AFT cage in the AFX structure (530 Å^3) and comparing that with an estimated volume obtained from bulk density for a substituted anthracene molecule (610 Å^3). At this point, only cracking reactions can then proceed in the larger AFT cage, and any carbon buildup has to occur in the smaller GME cage.

dx.doi.org/10.1021/cs300558x | ACS Catal. 2012, 2, 2490−2495

This difference in the coking mechanism is also observed in the average molecular weights of the occluded organic species in Table 2. LEV and CHA continue increasing average molecular weight of the hydrocarbon pool as the reaction deactivates from the point of maximum propylene selectivity while the net pool stays approximately constant during the deactivation of the AFX structure. This again suggests that the AFX is deactivating due to pore blockage.

Si/Al Variation Study. Variations in the Si/Al ratio of the CHA and in LEV materials caused alterations in the primary crystallite sizes. The results are shown in Figure 6. Data in Figure 7

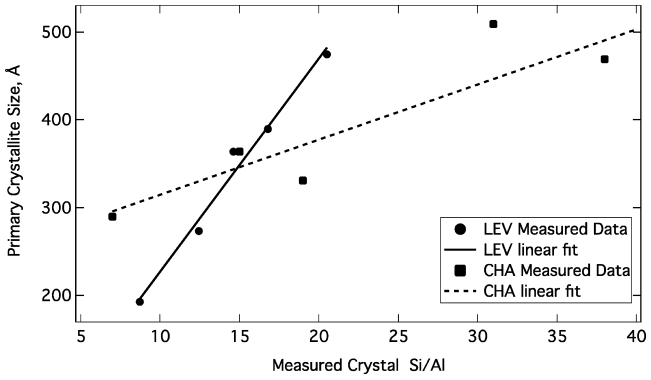

Figure 6. Primary crystallite size variations versus crystal Si/Al. The linear fits have R^2 = 0.98 for LEV and R^2 = 0.88 for CHA.

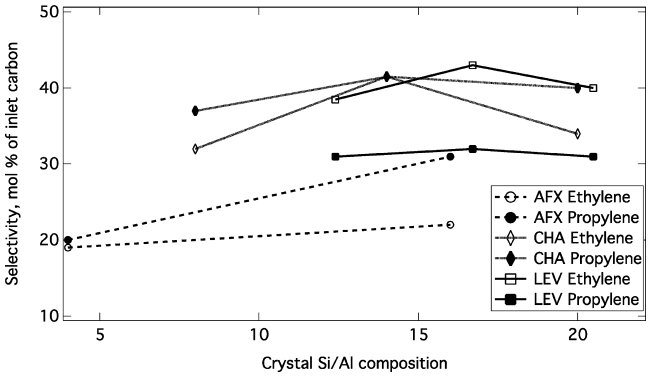

Figure 7. Selectivities toward ethylene and propylene for LEV, CHA, and AFX at different Si/Al contents.

summarize the reaction selectivities as a function of the Si/Al ratio. The data suggest that a Si/Al ratio between 14 and 17 gives higher selectivity to propylene for all three materials. The data show the importance of having the Si/Al ratio of the sample above a critical value (based on these data above 12), otherwise resulting in rapid deactivation and poor selectivities. This is most apparent in the AFX structure, because a higher Al content resulted in poor selectivity toward both ethylene and propylene.

CONCLUSION

Zeolites with the LEV, CHA, and AFX frameworks were used to study the effect of the cage size on the selectivity toward lower olefins in the methanol-to-olefins reaction. All these materials had cavities that were accessible through 8-membered ring windows, but with cavities of differing lengths. The aggregate crystal size, primary crystallite size, and the Si/Al ratio were kept constant to study the effect of framework alone. Reaction testing of these catalysts showed that the selectivity toward ethylene increased with a decrease in the cage size. Propylene selectivity was highest with the CHA framework. The AFX material had the worst carbon yield and catalyst lifetime, but it also had the lowest amount of carbon deposited after complete deactivation, suggesting that there was pore blockage preventing further reaction. This interpretation is consistent with the analysis of the occluded organics, which showed that the AFX material formed large three-ring aromatics at maximum propylene selectivity, before the formation of smaller aromatics that filled the GME cage. Variation of the Si/Al ratio shows that the maximum selectivities are obtained at a Si/Al ratio of 14−17.

ASSOCIATED CONTENT

Supporting Information

Further characterization of the synthesized materials as well as occluded organic analyses. This information is available free of charge via the Internet at http://pubs.acs.org/.

AUTHOR INFORMATION

Corresponding Author

*E-mail: mdavis@cheme.caltech.edu.

Present Address

⊥Instituto de Tecnología Química, UPV-CSIC, Universidad Politécnica de Valencia, Consejo Superior de Investigaciones Científicas, Valencia, Spain 46022

Notes

The authors declare no competing financial interest.

ACKNOWLEDGMENTS

The authors thank The Dow Chemical Company for financial support of this work. The authors also thank Chengli Zu and Suzanne Lehr of Analytical Sciences at The Dow Chemical Company for their assistance with the GC/MS work.

REFERENCES

(1) Vora, B; Marker, T. L.; Barger, P. T.; Nilsen, H. R.; Kvisle, S.; Fuglerud, T. *Stud. Surf. Sci. Catal.* **1997**, *107*, 87−98.
(2) Dahl, I. M.; Kolboe, S. *Catal. Lett.* **1993**, *20*, 329−336.
(3) Olsbye, U.; Svelle1, S.; Bjørgen, M.; Beato, P.; Janssens, T. V. W.; Joensen, F.; Bordiga, S.; Lillerud, K. P. *Angew. Chem.* **2012**, *51*, 5810−5831.
(4) Hereijgers, B. P.; Bleken, F.; Nilsen, M. H.; Svelle, S.; Lillerud, K.-P.; Bjørgen, M.; Weckhuysen, B. M.; Olsbye, U. *J. Catal.* **2009**, *264*, 77−87.
(5) Bjørgen, M.; Svelle, S.; Joensen, F.; Nerlov, J.; Kolboe, S.; Bonino, F.; Palumbo, L.; Bordiga, S.; Olsbye, U. *J. Catal.* **2007**, *249*, 195−207.
(6) Chang, C. D.; Silvestri, A. J. *J. Catal.* **1977**, *47*, 249−259.
(7) Chen, D.; Moljord, K.; Fuglerud, T.; Holmen, A *Microporous Mesoporous Mater.* **1999**, *29*, 191−203.
(8) Zones, S. Zeolite SSZ-13 and its method of preparation; U.S. Patent 4,544,538, 1985.
(9) Park, J.; Lee, J.; Kim, K.; Hong, S.; Seo, G. *Appl. Catal., A* **2008**, *339*, 36−44.
(10) Baerlocher, Ch.; McCusker, L. B.; Olson, D. H. *Atlas of Zeolite Framework Types*; Structure Commission of the International Zeolite Association, 6th ed.; Elsevier: London, 2007.
(11) Inoue, K.; Inaba, M.; Takahara, I.; Murata, K. *Catal. Lett.* **2010**, *136*, 14−19.
(12) Zhu, Q.; Kondo, J. N.; Ohnuma, R.; Kubota, Y.; Yamaguchi, M.; Tatsumi, T. *Microporous Mesoporous Mater.* **2008**, *112*, 153−161.
(13) Zones, S.; Van Nordstrand, R. A. *Zeolites* **1988**, *8*, 409−415.
(14) Archer, R. H.; Zones, S. I.; Davis, M. E. *Microporous Mesoporous Mater.* **2010**, *130*, 255−265.
(15) Fickel, D.; Lobo, R. *J. Phys. Chem. C* **2009**, *114*, 1633−1640.
(16) Scherrer, P. *Göttinger Nachrichten Gesell.* **1918**, *2*, 98−100.